

# Tuna and billfish larval distributions in a warming ocean

Hiroataka Ijima,<sup>1\*</sup> Marko Jusup,<sup>1</sup>

<sup>1</sup>Fisheries Resources Institute, Japan Fisheries Research and Education Agency,  
Yokohama 236-8648, Japan

\*To whom correspondence should be addressed; E-mail: [ijima\\_hiroataka69@fra.go.jp](mailto:ijima_hiroataka69@fra.go.jp).

**Tuna and billfish are charismatic pelagic fishes attracting considerable scientific attention due to their ecophysiological and socioeconomic importance. However, the knowledge of their basin-wide spawning and larval habitats, especially in a warming ocean, is limited. We use the largest available dataset on tuna and billfish larvae in the Pacific Ocean to build a geostatistical species-distribution model with high explanatory power. The results reveal the spatial distribution of tuna and billfish larvae through all seasons across the Pacific. The model also identifies the optimal temperature ranges for nine major species and assesses the potential impact of ocean warming on larval distributions. We additionally present evidence that environmental variables, such as pH, phosphate concentration, and sea-surface height, exert secondary effects on larval distributions that warrant further investigation. Our findings make a quantum leap in understanding the ecophysiology of tuna and billfish, providing valuable information for future conservation efforts.**

## Introduction

Tuna and billfish are known for their extraordinary physique that captivates public and scientific imagination alike. Tuna, for example, have motivated a large body of work on their swimming (1–3) and metabolic (4–8) performance, inspiring even the design of biomimetic underwater autonomous vehicles (9). The ability to perform at high levels enables tuna and billfish to populate all oceans and migrate over extreme distances (1, 10, 11), as well as occupy the ecological niche of apex marine predators (1, 12, 13).

The ecophysiology of tuna and billfish underpins their socioeconomic status. Their muscular bodies and cosmopolitan distribution make them a highly sought-after catch. The tuna fishery is thus the most valuable one in monetary terms (14, 15), whereas billfish are both highly prized as gamefish and subject to regional commercial fishing (16). The global exploitation of tuna and billfish has raised concerns about overfishing and the sustainability of wild stocks (17, 18). To address these concerns, major fishing powers are coordinating management and conservation efforts through the operations of regional fisheries management organizations (RFMOs), with the goal of establishing sustainable tuna and billfish fisheries.

An increasingly complete understanding of fish ecophysiology is essential for effective management and conservation of wild stocks (19). Ecophysiology provides insight into how functional traits contribute to fisheries-driven population risks (20, 21) and can help identify targets for monitoring that simplify population health assessments (22–24). Despite its importance, the ecophysiology of tuna and billfish is incomplete, particularly with regards to their basin-wide spawning and larval habitats in a warming ocean (25, 26). We address this gap in knowledge using a larval survey dataset for the period from 1960 to 1985 collected across the Pacific Ocean (Figure 1a). The dataset, previously described in the literature (27, 28), includes records of species, geolocation, effort (in  $\text{m}^3 \text{min}^{-1}$ ), and sea-surface temperature (SST). Our analysis

focuses on nine tuna and billfish species identified with confidence, out of the 24 species or multi-species groups documented in the dataset (Figure 1b).

The analysis in this study extracts new knowledge from the larval-survey dataset by using geostatistical species-distribution modelling. The process involved hypothesizing and fitting candidate models, followed by selecting the model that best balances explanatory power and simplicity (Supporting Table 1; see also Supporting Figures 1–5). The selected model passed the diagnostic testing (Supporting Figures 6–8). The modelling results provide unique insights into the spatial and seasonal variations of tuna and billfish larvae distribution, the impact of SST on larval densities, the influence of environmental variables on larval distributions, and more. The mathematical details of the model are outlined in the Methods section, and the numerical implementation can be accessed online (see Code availability).

## Results

**Reference larval distributions.** Our primary focus is on the impact of SST on tuna and billfish larvae in the Pacific Ocean. It is beneficial, however, to first examine the spatial and seasonal variations of larval distributions as predicted by the model for the period of 1960-1985 (Figure 2). The larvae of yellowfin tuna, skipjack tuna, and blue marlin are widely distributed around the equatorial Pacific. These distributions experience seasonal changes with a northward shift during boreal warm months and a southward shift during austral warm months. The larvae of bigeye tuna, albacore tuna, swordfish, striped marlin, and sailfish occupy medium to small patchy areas in the Pacific. These areas undergo substantial seasonal changes, particularly away from the equator where the presence or absence of larvae is mostly correlated with warm or cold months. The larvae of Pacific bluefin tuna are unique. They gather exclusively in the northwestern Pacific during boreal spring and summer.

**Primary ocean-warming effects.** Varying ocean temperatures can cause the displacement of marine species (29–33). Accordingly, the rising SST trend in the Pacific (Figure 3a) is leading to changes in the distribution of tuna and billfish larvae. To understand these changes, our model predicts the larval response to SST for all studied species (Figure 3b; Table 1). The optimal temperature for the larvae of most species is between 25–30 °C. Only the larvae of blue marlin and sailfish can thrive at temperatures above 30 °C. Billfish have a wider temperature tolerance than tuna, which underpins a positive effect of rising SST on the density of blue-marlin, sailfish, and striped-marlin larvae, both under current conditions and during the 1997–98 El Niño event (Figure 3c). Swordfish and four tuna species experience a negative effect because of their relatively low optimal temperature or narrow temperature tolerance range compared to billfish larvae. Pacific bluefin tuna is exceptional among tunas due to the limited extent of its larval habitat, where SST has been approaching the optimum for the species in recent years (Figure 3d, e). This highlights the importance of a geospatially resolved analysis. Ocean temperature trends vary by location, and what counts is the trend at locations where larvae are likely to be found.

We used SST as the sole predictor in the model for two reasons. Firstly, to distinguish the primary effects of ocean warming on tuna and billfish larvae from the secondary effects mediated by other environmental variables, and secondly, to minimize input uncertainties because SST was the only variable surveyed together with the larvae. The model incorporates secondary effects into a latent spatial field (see Methods). The specific environmental variables shaping this field remain hidden without further analysis. Before such an analysis, however, we compare the relative strength of primary and secondary effects on larval densities. The results indicate that these effects are similar in magnitude (Figure 4a). The primary effects prevail in the central-Pacific longitudes (Figure 4b) and tropical latitudes (Figure 4c), whereas secondary effects prevail in the remaining 60–75 % of the study area, depending on the species. For this

reason, a more in-depth examination of the characteristics of the latent spatial field and its potential drivers is necessary.

**Secondary environmental effects.** Many but not all characteristics of the model-estimated latent spatial field for tuna and billfish larvae can be understood based on their phylogeny and life history. Apart from the idiosyncrasies of Pacific bluefin tuna, the latent spatial field for other studied species is either tropical tuna-like or marlin-like (Figure 5a). This distinction is based on a quantitative analysis using normalised mutual information as a measure of similarity between datasets (Figure 5b). We favoured normalised mutual information over simple cross-correlation because the former has the potential to capture non-linear associations that the latter cannot (34). A similarity network with link weights equal to normalised mutual information shows that species with the tropical tuna-like latent spatial field are yellowfin tuna, bigeye tuna, skipjack tuna, and surprisingly, sailfish. Species with the marlin-like latent spatial field are striped marlin, blue marlin, swordfish, and surprisingly, albacore tuna. These two inconsistencies with phylogeny, sailfish and albacore tuna, suggest that the same adaptations may apply to phylogenetically distant species.

To identify the potential drivers of the secondary effects on tuna and billfish larvae, we analysed 10 environmental variables for association with the latent spatial field. The variables, including eddy kinetic energy, mixed-layer depth, sea-surface-height variability, dissolved molecular oxygen, carbon dioxide, salinity, sea-water pH, nitrate, phosphate, and chlorophyll, account for various geophysical, geochemical, and bioproductivity factors. We resorted to mutual information once more and found that sea-water pH, phosphate, and sea-surface-height variability are strongly associated with the latent spatial field (Figure 5c), especially for species with the marlin-like latent spatial field. The direction of these associations, positive or negative, is the same across all species. Taken together, the results suggest that striped marlin, blue marlin,

swordfish, and albacore tuna may be somewhat more susceptible to ocean acidification, evasive of high-phosphate areas, and attracted to elevated sea surface than yellowfin tuna, bigeye tuna, skipjack tuna, and sailfish. Strong associations, however, should not be mistaken for causality, implying that further studies are needed to understand the underlying mechanisms.

## **Discussion**

Our aim was to expand the ecophysiological understanding of tuna and billfish with emphasis on mapping larval habitats and quantifying the response of larvae to ongoing ocean warming. We achieved this by developing a geostatistical species-distribution model with high explanatory power based on the most comprehensive dataset on tuna and billfish larvae in the Pacific Ocean to date (27, 28). Our study is among the first of its kind, not because of data unavailability, but due to recent advancements in geostatistical species-distribution modelling (35) and the computational resources required to generate basin-wide results. We used a workstation with 128 CPU cores and 1 TB of memory during the modelling process.

The model we developed is versatile. Conservationists, for example, might use it to determine the distribution of larval diversity in the Pacific (Figure 6). The distribution reveals a distinctive divide in larval diversity across 140° W longitude, and a hotspot of diversity south of Japan during boreal spring and summer. These patterns align with established distributions of SST (36) and sea-surface-height variability (37), with the latter being the environmental variable most closely linked to the model-generated latent spatial field and thereby larval densities.

It is crucial to take into account multiple environmental variables. We project ocean warming to have a positive impact on bluefin-tuna, striped-marlin, blue-marlin, and sailfish larvae, whereas the rest of the species studied are expected to be negatively affected. These are, however, primary effects that may be amplified or suppressed by other environmental variables. Our analysis highlights sea-water pH as one important variable, which we link to lower larval den-

sities as acidity increases. Given that ocean warming is driven by rising CO<sub>2</sub> concentration in the atmosphere, which also contributes to ocean acidification (38), there is uncertainty around the extent to which the positive temperature effects can be realized. Moreover, five of the nine species studied appear to be at risk from both rising SST and declining sea-water pH, creating a double jeopardy for their well-being.

Our analysis also underscores the importance of phosphate availability as an environmental variable. We link more phosphate to reduced larval densities. Indeed, the larval diversity hotspot south of Japan coincides with one of the most phosphate-deficient regions in the Pacific Ocean (39). This is intriguing because phosphorus is widely considered the limiting nutrient for primary production (40), even if recent research suggests a more nuanced picture (39). It has been argued that tuna and billfish larvae may have a reduced dependence on primary production due to substantial larval cannibalism (41), and that hatching in areas with less primary production may provide some protection from predators (42). However, a causal relationship between phosphate availability and larval density remains largely unclear.

Finally, our analysis highlights the importance of sea-surface-height variability as an environmental variable. We link higher variability to increased larval densities. The impact of sea-surface height on tuna and billfish larval abundance has been previously documented (43, 44), but the underlying causality remains as elusive as for phosphorus. The arguments connecting negative sea-surface-height anomalies with upwelling and primary production (44) are contradicted by our result showing no effect of chlorophyll concentration on larval densities. Overall, causal relationships between environmental variables and larval densities remain vague, presenting a number of crucial research questions for future studies. A natural starting point to pursuing these questions would be to consider environmental variables emphasised by mutual information. One should keep in mind, however, that mutual information is akin to cross-correlation in that both fall short of guaranteeing the presence of underlying causality even

between two strongly associated quantities.

## Methods

**Preliminaries.** The present study’s purpose is to add value to the largest available dataset on tuna and billfish larvae in the Pacific Ocean by extracting from the dataset new fundamental and actionable knowledge on larval ecophysiology. Our attempt at achieving such a purpose was predicated on building a geostatistical species-distribution model that best balances explanatory power and mathematical parsimony. The term ‘explanatory power’ refers to the ability of the model to associate patterns in the dataset with predictor variables accounted for manifestly, and latent spatial factors standing in for missing predictors. The term ‘mathematical parsimony’ refers to keeping the model formulation as simple as possible without sacrificing explanatory power to a significant degree.

Our modelling decisions were guided by the fact that biogeochemical interactions on an ocean-wide scale form a complex system. A full geostatistical description of such a system is conceptually hard because of many moving parts, and practically challenging because of vast data requirements. This implies that even models with many predictor variables would still likely miss important predictors, which is why we decided to err on the side of simplicity. Specifics are outlined hereafter and include the model’s mathematical formulation, as well as implementational details and custom definitions. Data sources are listed in Data availability.

**Model formulation.** We built our geostatistical species-distribution model in three distinct steps. First, we assumed that larval density at spatio-temporal point  $i$  for species  $j$  is a random variable following the Tweedie distribution

$$y_{ij} \sim \mathcal{T}w(\mu_{ij}, p_j, \phi_j), 1 < p_j < 2 \wedge \phi_j > 0, \quad (1)$$



where  $\mu_{ij}$  is the mean,  $p_j$  is the power parameter, and  $\phi_j$  is the dispersion parameter. All three parameters jointly determine the distribution's variance  $\text{var}[y_{ij}] = \phi_j \mu_{ij}^{p_j}$ . The Tweedie distribution is characterised by the non-negative real support  $[0, +\infty)$  on which there is a probability mass concentrated at zero, followed by an exponentially decreasing profile away from zero. These characteristics naturally fit applications such as ours, in which many zero measurements are accompanied by occasional positive outcomes whose likelihood declines with size.

The second step in model building was to represent the mean larval density at point  $i$  for species  $j$  as

$$\mu_{ij} = \exp(\mathbf{X}_i \boldsymbol{\beta}_j + \mathbf{Z}_i \mathbf{L}_j), \quad (2)$$

where  $\mathbf{X}_i$  is a row vector of observed predictor-variable values at point  $i$  and  $\boldsymbol{\beta}_j$  is a column vector of model coefficients for species  $j$ . The row vector  $\mathbf{Z}_i$  is a latent spatial analogue of the vector  $\mathbf{X}_i$ , incorporating further mathematical structure relevant for modelling larval densities. The column vector  $\mathbf{L}_j$  is a latent spatial analogue of the vector  $\boldsymbol{\beta}_j$  whose components  $l_j^f$  are  $l_j^f \neq 0$  if  $f < j$ ,  $l_j^f = 1$  if  $f = j$ , and  $l_j^f = 0$  if  $f > j$ , where  $f$  indexes layers of the latent spatial field.

The final step in model building was to assign mathematical structure to the vector  $\mathbf{Z}_i$ . The components  $z_i^f$  of this vector are interpolated using  $z_i^f = \mathbf{A}_{[i]} \mathbf{U}_{\{i\}}^f$ , where  $[i]$  and  $\{i\}$  respectively refer to the geolocation and the timestamp of point  $i$ . The row vector  $\mathbf{A}_{[i]}$  contains the barycentric coordinates of point  $i$  arising from a Delaunay triangulation of the study area (45). The Delaunay triangulation covers the study area with a set of nodes, indexed by  $k$ , at which we keep track of the components  $u_{k,t}^f$  of each layer  $\mathbf{U}_{\{i\}}^f$  of the latent spatial field.

We assumed that the latent spatial field is temporally and spatially auto-correlated. The former is captured by

$$u_{k,t}^f = \sum_{s=1}^4 \rho_s^f u_{k,t-s}^f + \omega_{k,t}^f, \quad (3)$$

where  $\rho_s^f$  are auto-regressive coefficients that determine the temporal auto-correlation structure

of the overall model. The remaining term  $\omega_{k,t}^f$  represents a realisation at node  $k$  and time  $t$  of the Gaussian Markov random field  $\omega^f \sim \text{GMRF}(0, \Sigma^f)$  whose covariance matrix  $\Sigma^f$  stores the spatial auto-correlation structure of the model. To satisfy the Markovian property, the covariance between any two points distance  $d$  apart is given by the Matérn covariance function

$$M_{\text{cov}}(d) = \frac{\sigma^2}{2^{\nu-1}\Gamma(\nu)} (\kappa d)^\nu K_\nu(\kappa d), \quad (4)$$

where  $\Gamma(\cdot)$  is the gamma function,  $K_\nu(\cdot)$  is the modified Bessel function of the second kind,  $\sigma^2$  is the variance, and  $\nu$  and  $\kappa$  are positive parameters.

**Implementation and custom definitions.** We estimated the model's parameters using the maximum-likelihood method. This method entails choosing the parameter values that maximise the log-likelihood of observing the dataset at hand. The log-likelihood is

$$\begin{aligned} \log \mathcal{L} &= \sum_i \sum_j \log p(y_{ij} | \beta_j, \mathbf{L}_j, \rho_s, p_j, \phi_j; \Sigma^f) \\ &= \sum_i \sum_j \log \int p(y_{ij} | \beta_j, \mathbf{L}_j, \rho_s, p_j, \phi_j; \omega^f) \\ &\quad \times p(\omega^f | \Sigma^f) \prod_f d\omega^f, \end{aligned} \quad (5)$$

where  $p(\cdot|\cdot)$  signify probability density functions as per model definitions. Specifically,  $p(y_{ij} | \beta_j, \dots; \omega^f)$  is the probability density function for the Tweedie distribution  $\mathcal{T}\omega(\mu_{ij}, p_j, \phi_j)$ , whereas  $p(\omega^f | \Sigma^f)$  is the joint probability density function for a set of independent multivariate normal distributions with the covariance matrices  $\Sigma^f$ . The log-likelihood was, due to its complexity, maximised numerically with the R package TMB (46).

An important modelling decision was to restrict the model's predictor variables solely to sea-surface temperature (SST). The reasons for this are twofold. First, the product  $\mathbf{X}_i \beta_j$  isolates the primary effect of SST on mean larval densities, whereas the product  $\mathbf{Z}_i \mathbf{L}_j$  subsumes the secondary effects of latent spatial factors that stand in for missing predictors, presumably

key environmental variables. Second, SST had been the only quantity measured during the original larval survey. The SST dataset is therefore free of input uncertainties inherent in processed datasets. We employed processed datasets from widely trusted oceanographic sources to identify potential drivers of the latent spatial field rather than as explicit predictor variables in the model. We relied on mutual information for this purpose. Mutual information, although less ubiquitous than cross-correlation, is a well-documented measure of both linear and non-linear associations between variables (34).

The product  $\mathbf{X}_i\boldsymbol{\beta}_j$  is structured as follows. We assumed that for each species there is an optimal temperature  $\text{SST}_j^0$ , deviations from this temperature  $\Delta\text{SST}_{ij} = \text{SST}_i - \text{SST}_j^0$  cause larval densities to decrease, and the decrease is symmetric with respect to  $\Delta\text{SST}_{ij}$ . A simple functional form satisfying these assumptions is  $\mathbf{X}_i\boldsymbol{\beta}_j = \beta_{j,0} + \beta_{j,1}(\Delta\text{SST}_{ij})^2$ , with  $\beta_{j,1} < 0$ . For species  $j$ , therefore, the maximum of the mean larval density is  $\exp(\beta_{j,0})$ , whereas a fractional decline of the mean larval density given an arbitrary SST deviation is  $\exp[\beta_{j,1}(\Delta\text{SST}_j)^2]$ .

We used some custom definitions to quantify the effects of ocean warming on tuna and billfish larvae. Once the estimation of  $\boldsymbol{\beta}_j$  and  $\mathbf{L}_j$  is completed, the individual terms of Eq. (2) can be treated as continuous functions of location  $\mathbf{r}$  over the study area and time  $t$ :  $\mu_{ij} \mapsto \mu_j(\mathbf{r}, t)$  is the mean larval density,  $\exp(\mathbf{X}_i\boldsymbol{\beta}_j) \mapsto \mu_j^1[\text{SST}(\mathbf{r}, t)]$  is its primary temperature-dependent component, and  $\exp(\mathbf{Z}_i\mathbf{L}_j) \mapsto \mu_j^2[\text{LSF}(\mathbf{r}, t)]$  is its secondary environment-dependent component. The mean larval density for the reference period 1960-85 is obtained by time-averaging SST to  $\text{SST}_{\text{ref}}(\mathbf{r})$  and the latent spatial field to  $\text{LSF}_{\text{ref}}(\mathbf{r})$ , thus eliminating time dependence

$$\mu_{j,\text{ref}}(\mathbf{r}) = \mu_j^1[\text{SST}_{\text{ref}}(\mathbf{r})]\mu_j^2[\text{LSF}_{\text{ref}}(\mathbf{r})]. \quad (6)$$

The reference larval mass is then the volume integral over the study area  $M_{j,\text{ref}} = \int \mu_{\text{ref}}(\mathbf{r})d^3\mathbf{r}$ .

Taking the difference  $\Delta\mu_j^1[\text{SST}(\mathbf{r}, t)]$  between  $\mu_j^1[\text{SST}(\mathbf{r}, t)]$  and  $\mu_j^1[\text{SST}_{\text{ref}}(\mathbf{r})]$  isolates and tracks through time the effects of ocean warming on larval densities relative to the reference

period. The magnitude of this difference, however, is important only where larvae is likely to be found. We therefore calculated a density-weighted aggregate effect of SST on species  $j$  as

$$AE_j = \frac{1}{M_{j,\text{ref}}} \int \mu_{j,\text{ref}}(\mathbf{r}) \Delta \mu_j^1[\text{SST}(\mathbf{r}, t)] d^3\mathbf{r}. \quad (7)$$

The fact that the mean larval density,  $\mu_j(\mathbf{r}, t)$ , is separable into a primary temperature-dependent component,  $\mu_j^1[\text{SST}(\mathbf{r}, t)]$ , and a secondary environment-dependent component,  $\mu_j^2[\text{LSF}(\mathbf{r}, t)]$ , allows identifying which of the components dominates at spatio-temporal location  $(\mathbf{r}, t)$ . A way to achieve this is to form a ratio of contributions

$$CR_j(\mathbf{r}, t) = \frac{\mu_j^1[\text{SST}(\mathbf{r}, t)]}{\mu_j^2[\text{LSF}(\mathbf{r}, t)]}. \quad (8)$$

The values  $0 < CR_j(\mathbf{r}, t) < 1$  signal that primary ocean-warming effects contribute to larval densities more than secondary environmental effects, whereas the values  $CR_j(\mathbf{r}, t) > 1$  signal the opposite.

To quantify diversity at location  $\mathbf{r}$ , we defined a diversity index

$$DI(\mathbf{r}) = \sum_j \mathbb{1}_{\{\mu_{j,\text{ref}}(\mathbf{r}') > 0\}}(\mathbf{r}), \quad (9)$$

where  $\mathbb{1}_A(\mathbf{r})$  is an indicator function such that  $\mathbb{1}_A(\mathbf{r}) = 1$  if  $\mathbf{r} \in A$  and  $\mathbb{1}_A(\mathbf{r}) = 0$  otherwise. The quantity  $DI(\mathbf{r})$  is a simple counter of positive reference larval densities at a chosen location.

**Data availability.** The data on larval abundance are publicly accessible from Zenodo at <https://doi.org/10.5281/zenodo.6592148>. The data on sea-surface temperature (SST) measured together with larval abundance and used for model learning are a property of the government of Japan; requests for access should be directed at the corresponding author. The SST data used to predict the effects of ocean warming on tuna and billfish larvae are from the Hadley Centre Sea Ice and Sea Surface Temperature data set (HadISST) publicly accessible at <https://www.metoffice.gov.uk/hadobs/hadisst/>. The data on mixed

layer depth and salinity are publicly accessible from The World Ocean Atlas (WOA18) at <https://www.ncei.noaa.gov/access/world-ocean-atlas-2018/>. The data on sea surface height relative to geoid are publicly accessible from the NCEP Global Ocean Data Assimilation System (GODAS) at <https://psl.noaa.gov/data/gridded/data.godas.html>. The data on surface partial pressure of carbon dioxide in sea water, mole concentration of dissolved molecular oxygen in sea water, mass concentration of chlorophyll a in sea water, mole concentration of phosphate in sea water, sea water pH reported on total scale, and mole concentration of nitrate in sea water are publicly accessible from the Copernicus Marine Service Information at <https://marine.copernicus.eu/access-data>. The data on eddy kinetic energy are a part of the Archiving, Validation and Interpretation of Satellite Oceanographic (AVISO) data publicly accessible at <https://www.aviso.altimetry.fr/en/data/data-access.html>.

**Code availability.** The code developed for this analysis is publicly accessible from the Open Science Framework (OSF) at <https://doi.org/10.17605/OSF.IO/42HM8>.

## References and Notes

1. Watanabe, Y. Y., Goldman, K. J., Caselle, J. E., Chapman, D. D. & Papastamatiou, Y. P. Comparative analyses of animal-tracking data reveal ecological significance of endothermy in fishes. *Proc. Natl. Acad. Sci. USA* **112**, 6104–6109 (2015).
2. Shadwick, R. E. & Syme, D. A. Thunniform swimming: muscle dynamics and mechanical power production of aerobic fibres in yellowfin tuna (*Thunnus albacares*). *J. Exp. Biol.* **211**, 1603–1611 (2008).

3. Dewar, H. & Graham, J. Studies of tropical tuna swimming performance in a large water tunnel—energetics. *J. Exp. Biol.* **192**, 13–31 (1994).
4. Estess, E. E. *et al.* Bioenergetics of captive pacific bluefin tuna (*Thunnus orientalis*). *Aquaculture* **434**, 137–144 (2014).
5. Jusup, M., Klanjšček, T. & Matsuda, H. Simple measurements reveal the feeding history, the onset of reproduction, and energy conversion efficiencies in captive bluefin tuna. *J. Sea Res.* **94**, 144–155 (2014).
6. Jusup, M., Klanjšček, T., Matsuda, H. & Kooijman, S. A. L. M. A full lifecycle bioenergetic model for bluefin tuna. *PLOS One* **6**, e21903 (2011).
7. Korsmeyer, K. E. & Dewar, H. Tuna metabolism and energetics. *Fish Physiol.* **19**, 35–78 (2001).
8. Korsmeyer, K. E., Dewar, H., Lai, N. C. & Graham, J. B. The aerobic capacity of tunas: adaptation for multiple metabolic demands. *Comp. Biochem. Physiol.* **113**, 17–24 (1996).
9. Wainwright, D. K. & Lauder, G. V. Tunas as a high-performance fish platform for inspiring the next generation of autonomous underwater vehicles. *Bioinspir. Biomim.* **15**, 035007 (2020).
10. Reygondeau, G. *et al.* Biogeography of tuna and billfish communities. *J. Biogeogr.* **39**, 114–129 (2012).
11. Graham, J. B. & Dickson, K. A. Tuna comparative physiology. *J. Exp. Biol.* **207**, 4015–4024 (2004).
12. Kitchell, J. F., Boggs, C. H., He, X. & Walters, C. J. Keystone predators in the central Pacific. In Mecklenburg, C. W. (ed.) *Ecosystem Approaches for Fisheries Management*,

- vol. 16 of *Lowell Wakefield Fisheries Symposium*, 665–683 (University of Alaska Sea Grant College Program, 1999).
13. Olson, R. J. & Boggs, C. H. Apex predation by yellowfin tuna (*Thunnus albacares*): independent estimates from gastric evacuation and stomach contents, bioenergetics, and cesium concentrations. *Can. J. Fish. Aquat. Sci.* **43**, 1760–1775 (1986).
  14. McKinney, R., Gibbon, J., Wozniak, E. & Galland, G. Netting billions 2020: A global tuna valuation. The Pew Charitable Trusts (2020). Available at: <https://www.pewtrusts.org/-/media/assets/2020/10/nettingbillions2020.pdf>.
  15. Guillotreau, P., Squires, D., Sun, J. & Compeán, G. A. Local, regional and global markets: what drives the tuna fisheries? *Rev. Fish Biol. Fish.* **27**, 909–929 (2017).
  16. Holland, S. M., Ditton, R. B. & Graefe, A. R. An ecotourism perspective on billfish fisheries. *J. Sustain. Tour.* **6**, 97–116 (1998).
  17. Collette, B. B. *et al.* High value and long life—double jeopardy for tunas and billfishes. *Science* **333**, 291–292 (2011).
  18. Juan-Jordá, M. J., Mosqueira, I., Cooper, A. B., Freire, J. & Dulvy, N. K. Global population trajectories of tunas and their relatives. *Proc. Natl. Acad. Sci. USA* **108**, 20650–20655 (2011).
  19. Horodysky, A. Z., Cooke, S. J., Graves, J. E. & Brill, R. W. Fisheries conservation on the high seas: linking conservation physiology and fisheries ecology for the management of large pelagic fishes. *Conserv. Physiol.* **4**, cov059 (2016).

20. Murua, H., Rodriguez-Marin, E., Neilson, J. D., Farley, J. H. & Juan-Jordá, M. J. Fast versus slow growing tuna species: age, growth, and implications for population dynamics and fisheries management. *Rev. Fish Biol. Fish* **27**, 733–773 (2017).
21. Juan-Jordá, M. J., Mosqueira, I., Freire, J. & Dulvy, N. K. Population declines of tuna and relatives depend on their speed of life. *Proc. Royal Soc. B Biol. Sci.* **282**, 20150322 (2015).
22. Haberle, I., Bavcevic, L. & Klanjcek, T. Fish condition as an indicator of stock status: Insights from condition index in a food-limiting environment. *Fish Fish* **n/a**, DOI: 10.1111/faf.12744 (2023).
23. Marn, N., Jusup, M., Kooijman, S. A. & Klanjscek, T. Quantifying impacts of plastic debris on marine wildlife identifies ecological breakpoints. *Ecol. Lett.* **23**, 1479–1487 (2020).
24. Ijima, H. *et al.* Effects of environmental change and early-life stochasticity on pacific bluefin tuna population growth. *Mar. Environ. Res.* **149**, 18–26 (2019).
25. Llopiz, J. K. & Hobday, A. J. A global comparative analysis of the feeding dynamics and environmental conditions of larval tunas, mackerels, and billfishes. *Deep. Sea Res. Part II Top. Stud. Ocean.* **113**, 113–124 (2015).
26. Reglero, P., Tittensor, D. P., Álvarez-Berastegui, D., Aparicio-González, A. & Worm, B. Worldwide distributions of tuna larvae: revisiting hypotheses on environmental requirements for spawning habitats. *Mar. Ecol. Prog. Ser.* **501**, 207–224 (2014).
27. Buenafe, K. C. V. *et al.* A global, historical database of tuna, billfish, and saury larval distributions. *Sci. Data* **9**, 423 (2022).
28. Nishikawa, Y. Average distribution of larvae of oceanic species of scombroid fishes, 1956-1981. Far Seas Fisheries Research Laboratory (1985). Series 12, 99 pp. Archived at: .



29. García Molinos, J. Global marine warming in a new dimension. *Nat. Ecol. Evol.* **4**, 16–17 (2020).
30. Oremus, K. L. *et al.* Governance challenges for tropical nations losing fish species due to climate change. *Nat. Sustain.* **3**, 277–280 (2020).
31. Burrows, M. T. *et al.* Ocean community warming responses explained by thermal affinities and temperature gradients. *Nat. Clim. Chang.* **9**, 959–963 (2019).
32. García Molinos, J. *et al.* Climate velocity and the future global redistribution of marine biodiversity. *Nat. Clim. Chang.* **6**, 83–88 (2016).
33. Burrows, M. T. *et al.* Geographical limits to species-range shifts are suggested by climate velocity. *Nature* **507**, 492–495 (2014).
34. Reshef, D. N. *et al.* Detecting novel associations in large data sets. *Science* **334**, 1518–1524 (2011).
35. Thorson, J. T. *et al.* Spatial factor analysis: a new tool for estimating joint species distributions and correlations in species range. *Methods Ecol. Evol.* **6**, 627–637 (2015).
36. Liu, J. *et al.* Eastern equatorial Pacific cold tongue evolution since the late Miocene linked to extratropical climate. *Sci. Adv.* **5**, eaau6060 (2019).
37. Kang, L., Wang, F. & Chen, Y. Eddy generation and evolution in the North Pacific Sub-tropical Countercurrent (NPSC) zone. *Chin. J. Ocean. Limnol.* **28**, 968–973 (2010).
38. Jacobson, M. Z. Studying ocean acidification with conservative, stable numerical schemes for nonequilibrium air-ocean exchange and ocean equilibrium chemistry. *J. Geophys. Res. Atmos.* **110** (2005).

39. Martiny, A. C. *et al.* Biogeochemical controls of surface ocean phosphate. *Sci. Adv.* **5**, eaax0341 (2019).
40. Tyrrell, T. The relative influences of nitrogen and phosphorus on oceanic primary production. *Nature* **400**, 525–531 (1999).
41. Reglero, P., Urtizbera, A., Torres, A. P., Alemany, F. & Fiksen, Ø. Cannibalism among size classes of larvae may be a substantial mortality component in tuna. *Mar. Ecol. Prog. Ser.* **433**, 205–219 (2011).
42. Bakun, A. & Broad, K. Environmental ‘loopholes’ and fish population dynamics: comparative pattern recognition with focus on El Niño effects in the Pacific. *Fish. Ocean.* **12**, 458–473 (2003).
43. Tawa, A., Kodama, T., Sakuma, K., Ishihara, T. & Ohshimo, S. Fine-scale horizontal distributions of multiple species of larval tuna off the Nansei Islands, Japan. *Mar. Ecol. Prog. Ser.* **636**, 123–137 (2020).
44. Rooker, J. R. *et al.* Distribution and habitat associations of billfish and swordfish larvae across mesoscale features in the Gulf of Mexico. *PLOS ONE* **7**, e34180 (2012).
45. Cameletti, M., Lindgren, F., Simpson, D. & Rue, H. Spatio-temporal modeling of particulate matter concentration through the SPDE approach. *AStA Adv. Stat. Anal.* **97**, 109–131 (2013).
46. Kristensen, K., Nielsen, A., Berg, C. W., Skaug, H. & Bell, B. M. TMB: Automatic differentiation and Laplace approximation. *J. Stat. Softw.* **70**, 1–21 (2016).
47. We are grateful to Hidetada Kiyofuji and Taketoshi Kodama for comments and insights. We acknowledge support from Research and assessment program for internationally managed

fisheries resources, the Fisheries Agency of Japan. M. J. was partly supported by the Japan Society for the Promotion of Science (JSPS) KAKENHI grant 21H03625.

47. H. I. and M. J. conceptualised research, interpreted results, and discussed implications. H. I. performed modelling work. M. J. wrote the manuscript.

Table 1: Sea-surface temperature (SST) optima for tuna and billfish larvae, and larval-density losses induced by SST deviating  $\pm 1$  °C from these optima. Blue-marlin and sailfish larvae thrive at exceptionally high SST. Billfish are less sensitive to suboptimal SST than tuna.

Species	Optimum, SST <sub>0</sub>	% larval loss at $\Delta$ SST = $\pm 1$ °C
Bluefin tuna	26.49	22.34
Bigeye tuna	27.87	16.98
Yellowfin tuna	28.05	16.83
Albacore tuna	28.13	17.12
Skipjack tuna	28.44	14.83
Swordfish	26.93	8.55
Striped marlin	28.91	9.67
Blue marlin	32.93	6.65
Sailfish	32.50	6.91

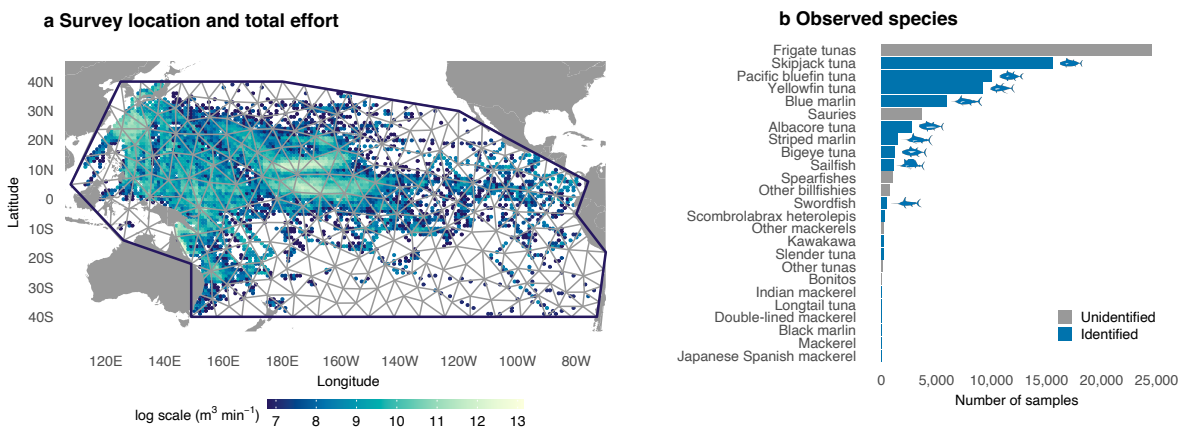


Figure 1: Larval-survey dataset. (a) The plot displays data points for the reference period from 1960 to 1985. Each data point contains records on geolocation, effort (in  $\text{m}^3 \text{min}^{-1}$ ), and sea-surface temperature (not shown), in addition to the observed larval species. The plot also displays a Delaunay triangulation of the area encompassing all larval-survey locations. The triangulation, comprising 277 nodes connected by edges whose maximum length is 1,250 km, defines the domain over which our geostatistical species-distribution model operates. (b) Larval surveys had observed a total of 24 individual species or multi-species groups. We focused our analyses on nine tuna and billfish species that had been discriminated with high confidence. Ordered by the number of samples, these are: skipjack tuna (*Katsuwonus pelamis*), Pacific bluefin tuna (*Thunnus orientalis*), yellowfin tuna (*Thunnus albacares*), blue marlin (*Makaira nigricans*), albacore tuna (*Thunnus alalunga*), striped marlin (*Kajikia audax*), bigeye tuna (*Thunnus obesus*), sailfish (*Istiophorus platypterus*), and swordfish (*Xiphias gladius*).

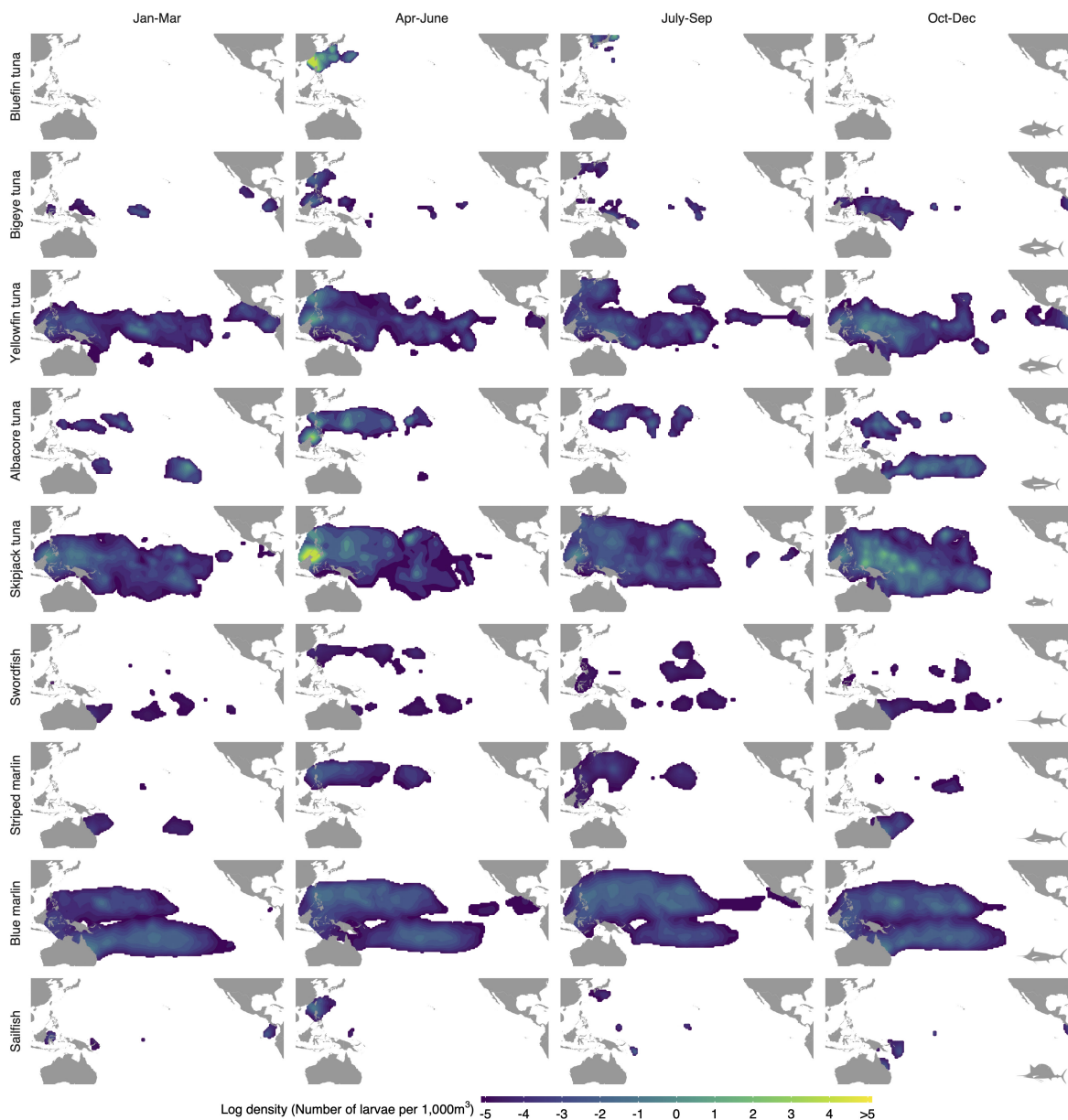


Figure 2: Seasonal tuna and billfish larval densities across the Pacific for the reference period 1960-85. In qualitative terms, we differentiate between (i) large-sized contiguous distributions of yellowfin-tuna, skipjack-tuna, and blue-marlin larvae, (ii) mid- to small-sized patchy distributions of bigeye-tuna, albacore-tuna, swordfish, striped-marlin, and sailfish larvae, and (iii) congregated distribution of Pacific bluefin-tuna larvae. Contiguous larval habitats are centred around the equator, but still, there is some seasonal variability mirrored in the northward (southward) pull during northern (southern) warm months. Patchier larval habitats are subject to even more pronounced seasonal changes, especially away from the equator where larvae tend to appear only during warm months. The Pacific bluefin-tuna larvae is exclusive to the northeastern Pacific in spring and, to a lesser degree, summer.

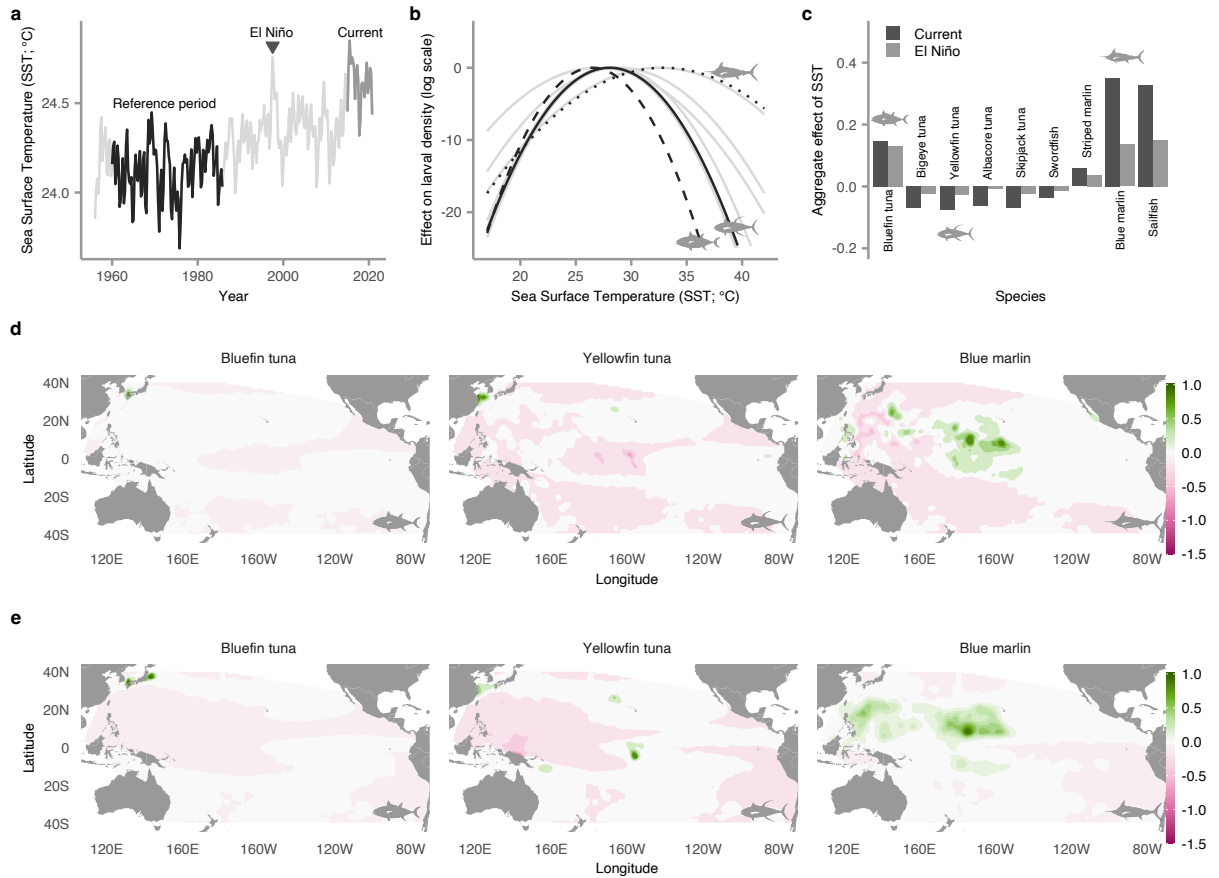


Figure 3: Geospatially resolved effects of rising sea-surface temperature (SST) on tuna and billfish larval densities. (a) SST in the Pacific Ocean has risen in recent decades. We used the 1960-85 period as a reference for building our geostatistical species-distribution model. (b) The model predicts the optimal SST for each species and the effect on larval density as SST deviates from the optimum. Pacific bluefin tuna, yellowfin tuna, and blue marlin are highlighted, representing low, moderate, and high optimal SST, respectively. (c) The model also predicts the aggregate impact of SST on larval density during the major El Niño event of 1997-98 and under current conditions, relative to the reference period. Pacific bluefin tuna, striped marlin, blue marlin, and sailfish are positively impacted, whereas bigeye tuna, yellowfin tuna, albacore tuna, skipjack tuna, and swordfish are negatively impacted. (d) The aggregate impact is based on a geospatially resolved analysis, illustrated here for the El Niño year for Pacific bluefin tuna (left), yellowfin tuna (middle), and blue marlin (right). The effect of SST at each location is weighted by reference larval density (shown in Figure 2) because rising SST is only relevant where larvae are likely to be found. Green and red shades respectively indicate areas where we can expect more or fewer larvae. (e) The same as panel d, but under the current conditions.

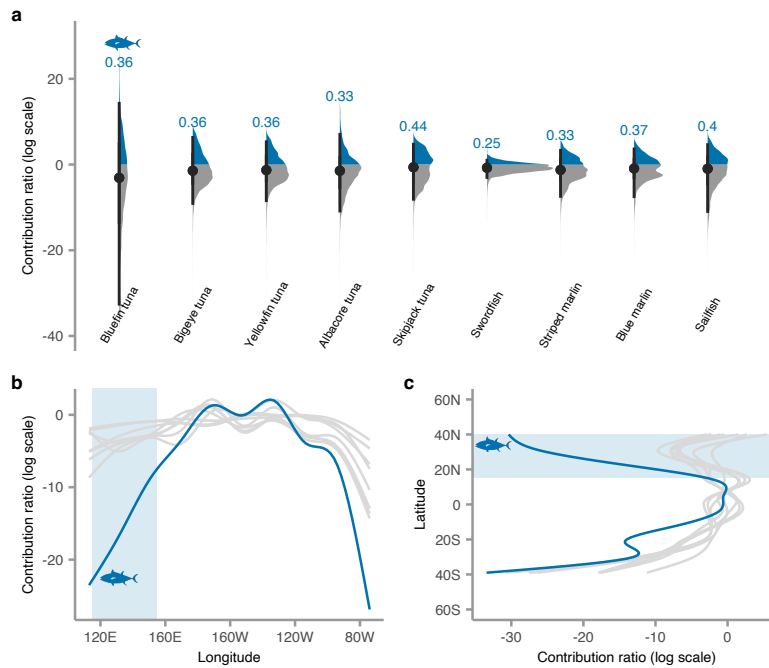


Figure 4: Comparing the relative strength of primary and secondary effects on tuna and billfish larval densities. (a) The primary effects, mediated by sea-surface temperature (SST), and the secondary effects, mediated by other environmental variables, are comparable in magnitude. We calculated the ratio of primary to secondary contributions to larval densities at all surveyed locations and displayed the distribution of results. The number on top of each distribution shows the percentage of locations where the primary effects prevail (b, c) Geographically, the primary effects prevail across the central-Pacific longitudes and tropical latitudes. The opposite holds in the remaining 60-75 % of the study area, which includes the extreme case of Pacific bluefin tuna in whose spawning habitat (light-blue shade) the secondary effects overshadow the primary ones.



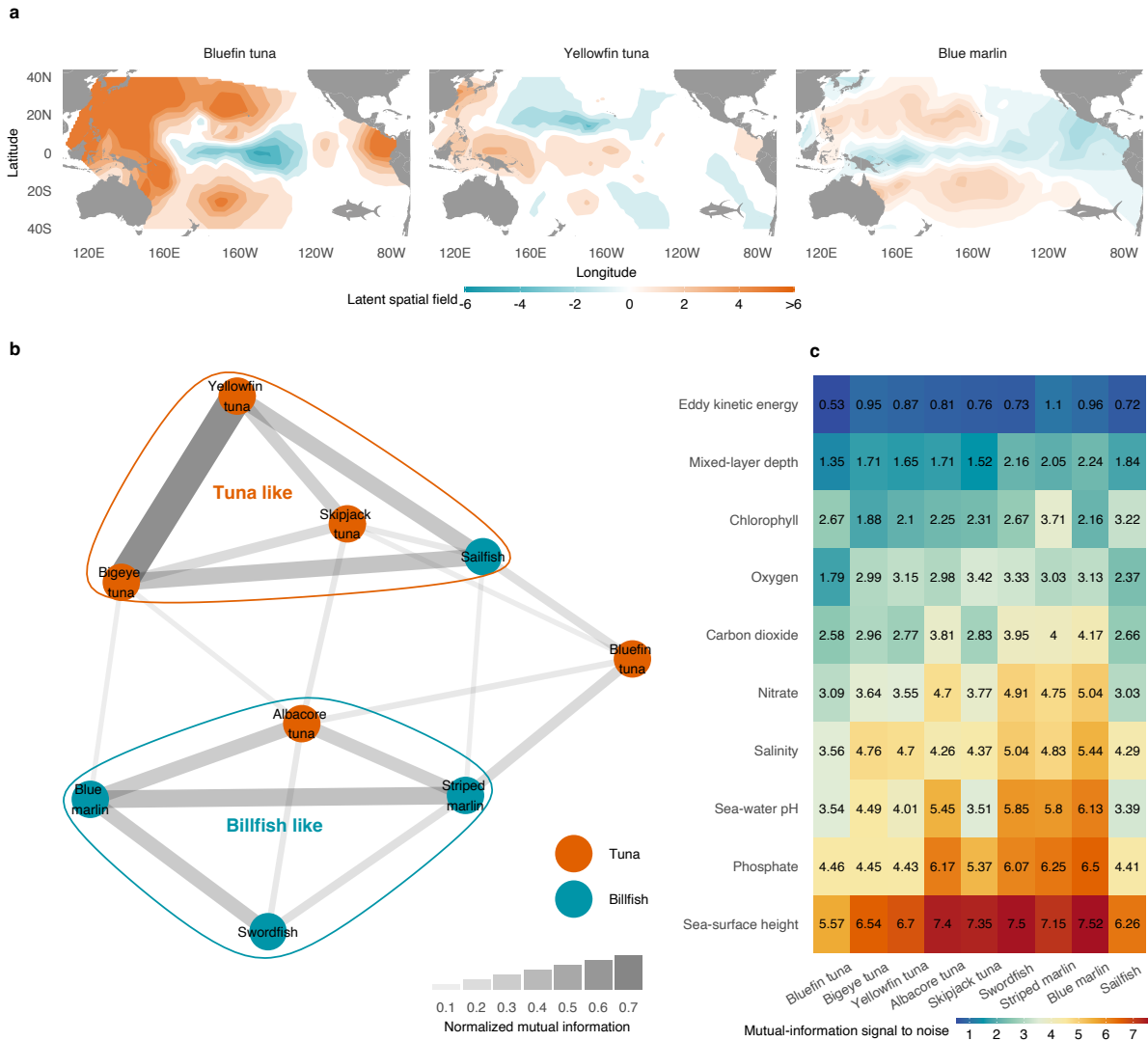


Figure 5: Characteristics and potential drivers of the latent spatial field. (a) Apart for the distinctive latent spatial field for Pacific bluefin tuna, others are either tropical tuna-like or marlin-like. Representative examples are yellowfin tuna and blue marlin, respectively. (b) A similarity network using normalized mutual information shows that species with the tropical tuna-like latent spatial field are bigeye tuna, yellowfin tuna, skipjack tuna, and sailfish. Species with the marlin-like latent spatial field are striped marlin, blue marlin, swordfish, and albacore tuna. Link width represents the normalized mutual information between linked species' latent spatial fields. Links with widths less than 0.1 are excluded. (c) Among the analysed environmental variables, sea-surface-height variability, phosphate concentration, and pH are most strongly associated with the latent spatial field. We defined signal to noise as the mutual information between the latent spatial field and an environmental variable divided by the same quantity when the environmental variable is randomly reshuffled.

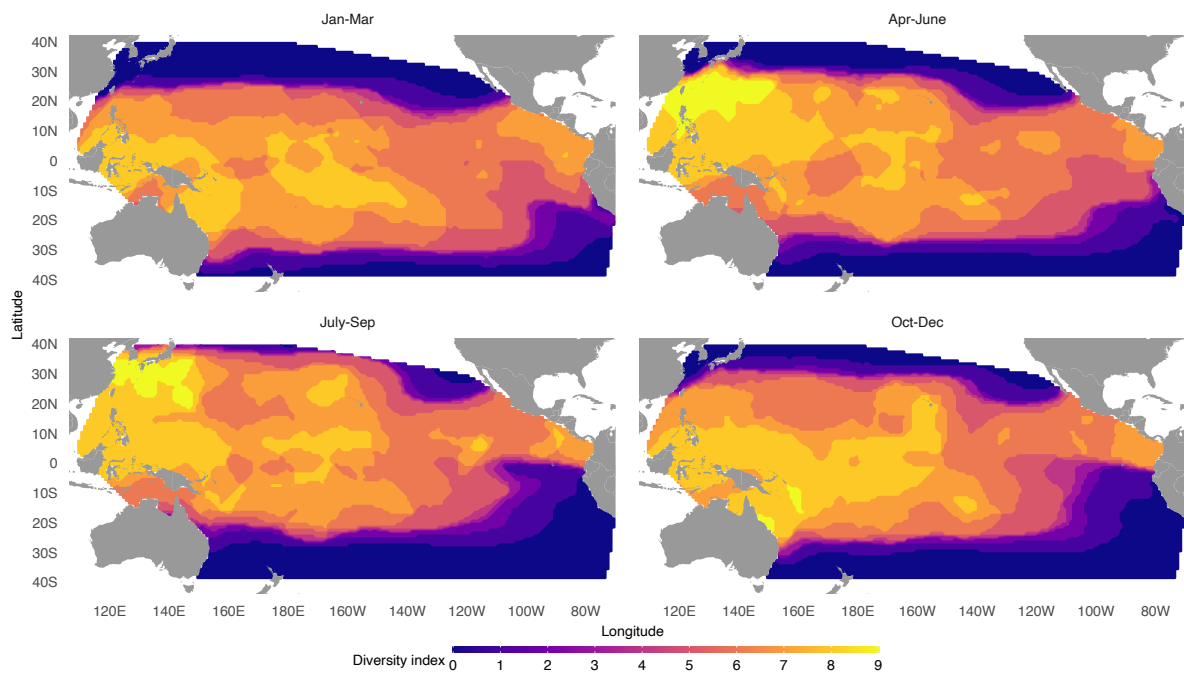


Figure 6: Larval diversity in the Pacific as inferred by our geostatistical species-distribution model. The western and central Pacific harbours noticeably more diversity than the eastern Pacific, with the overall distribution closely resembling the known distribution of sea-surface temperature (36). Additionally, there is a noticeable diversity patch south of Japan during the boreal spring and summer, which coincides with the known distribution of sea-surface-height variability (37).

Supporting material for:  
Tuna and billfish larval distributions in a warming  
ocean

Hiroataka Ijima,<sup>1\*</sup> Marko Jusup,<sup>1</sup>

<sup>1</sup>Fisheries Resources Institute, Japan Fisheries Research and Education Agency,  
Yokohama 236-8648, Japan

\*To whom correspondence should be addressed; E-mail: [ijima\\_hiroataka69@fra.go.jp](mailto:ijima_hiroataka69@fra.go.jp).

Supporting Table 1: Model selection. We hypothesised and tested 11 models of increasing complexity, expressing their (i) goodness of fit with the Akaike information criterion (AIC) obtained via maximum-likelihood estimation, and (ii) predictive power with the mean-square and mean-absolute errors (MSE and MAE, respectively) obtained via 10-fold cross-validation. Model complexity increased by adding more fixed-effect predictors, more latent spatial layers, or more auto-regressive terms. To avoid over-fitting and maximise predictive power, we chose the model with the lowest MSE and second lowest MAE, but only the fourth lowest AIC.

No.	Timestep	Predictors <sup>a</sup>	Layers <sup>b</sup>	AR terms <sup>c</sup>	NLL <sup>d</sup>	AIC <sup>e</sup>	MSE <sup>f</sup>	MAE <sup>g</sup>
1	yr	SST	1	1	55446	111003	1.2490	0.0875
2	yr	SST	2	1	53099	106330	1.2260	0.0841
3	qtr	SST	2	1	52314	104759	1.2460	0.0825
4	qtr	SST	2	4	52080	104304	1.2390	0.0823
5	qtr	SST, vTYP	2	4	51921	104003	1.2590	0.0821
6	qtr	SST, yr	2	4	50804	102202	1.2250	0.0804
7	qtr	SST	3	4	50614	101395	1.2190	0.0796
8	qtr	SST, yr	3	4	49928	100475	1.2200	0.0790
9 <sup>h</sup>	qtr	SST	4	4	50221	100632	1.2140	0.0786
10	qtr	SST, yr	4	4	49703	100047	1.2170	0.0786
11 <sup>i</sup>	qtr	SST	5	4	49983	100176	1.2170	0.0783

<sup>a</sup> Fixed-effect predictors: SST = sea-surface temperature (continuous), vTYP = vessel type (categorical), and yr = year (categorical)

<sup>b</sup> Number of latent spatial layers

<sup>c</sup> Number of auto-regressive coefficients

<sup>d</sup> Negative log likelihood

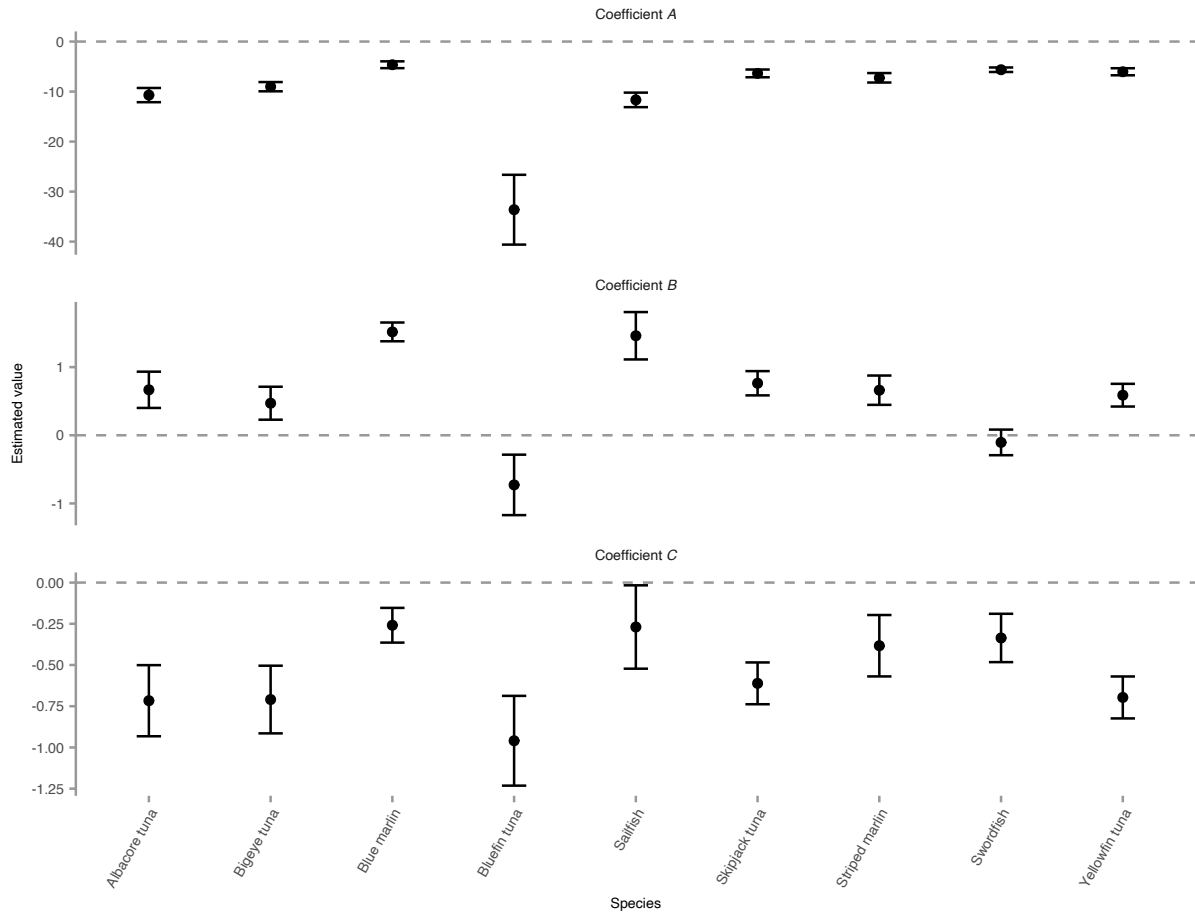
<sup>e</sup> Akaike information criterion

<sup>f</sup> Mean-square error of 10-fold cross-validation

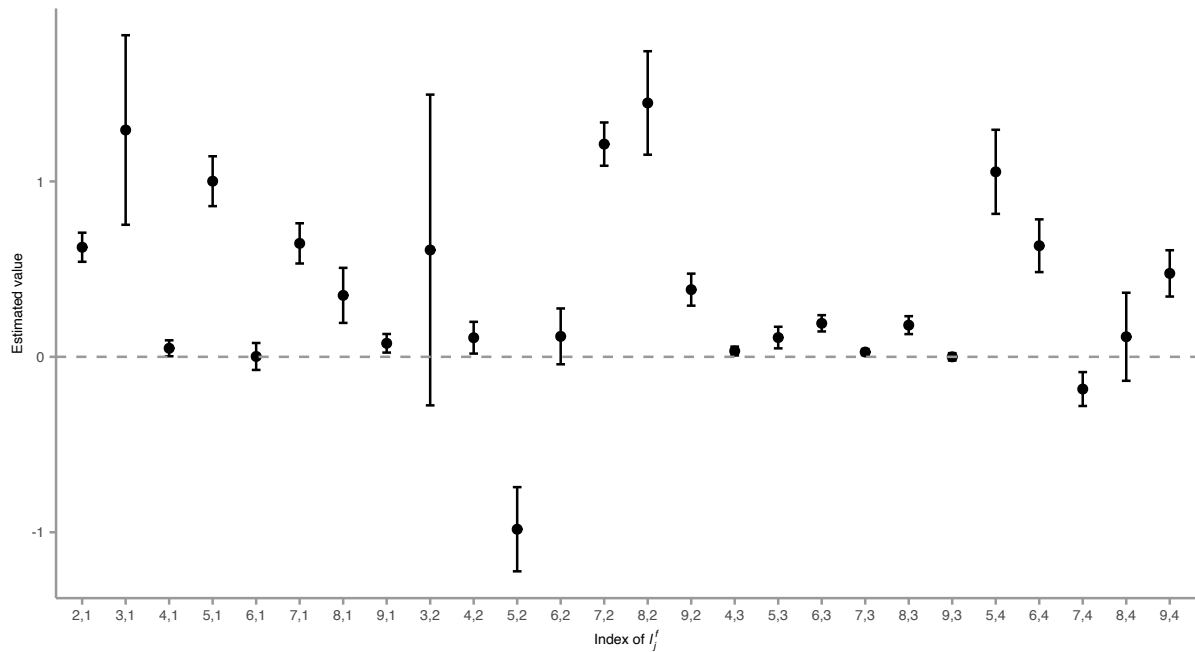
<sup>g</sup> Mean-absolute error of 10-fold cross-validation

<sup>h</sup> Selected model

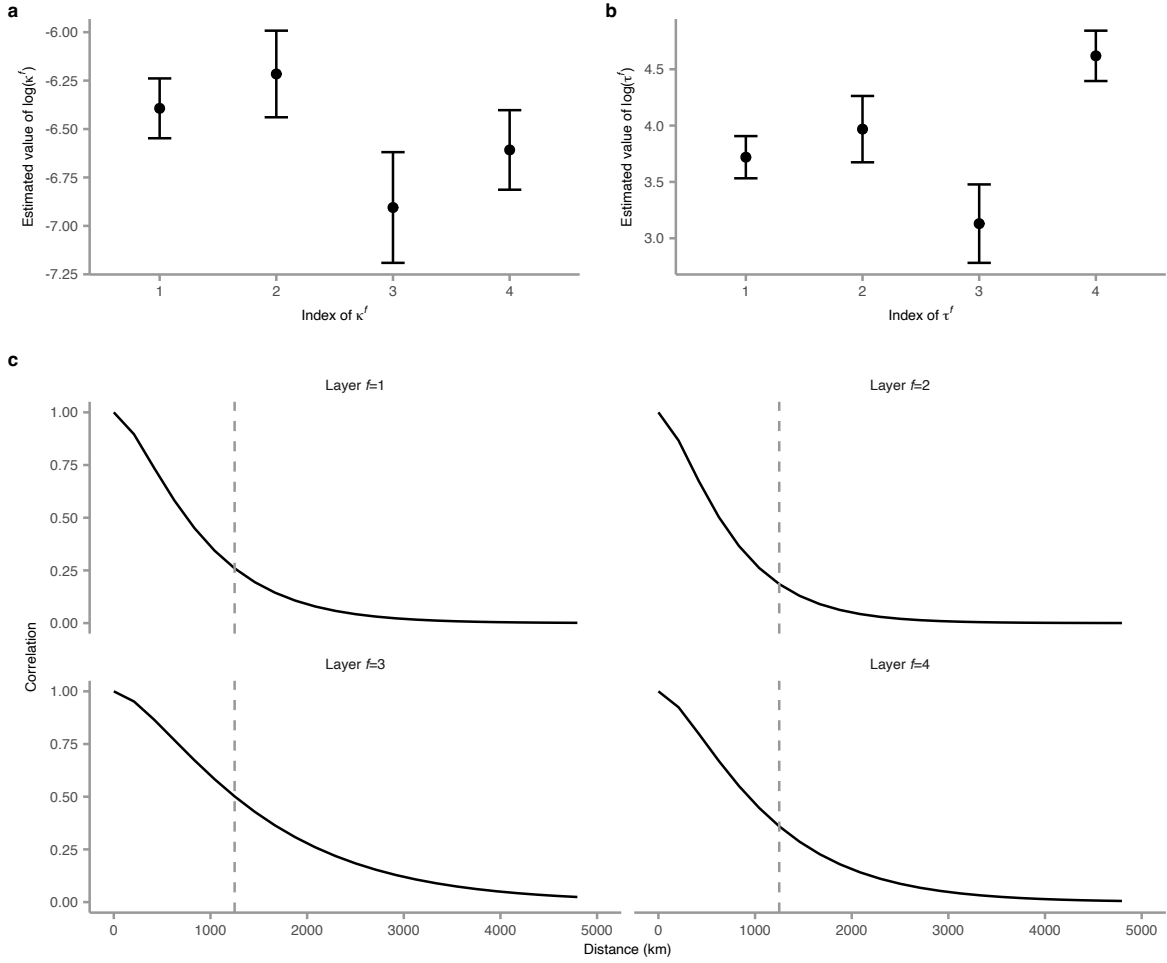
<sup>i</sup> Computing the Hessian matrix failed



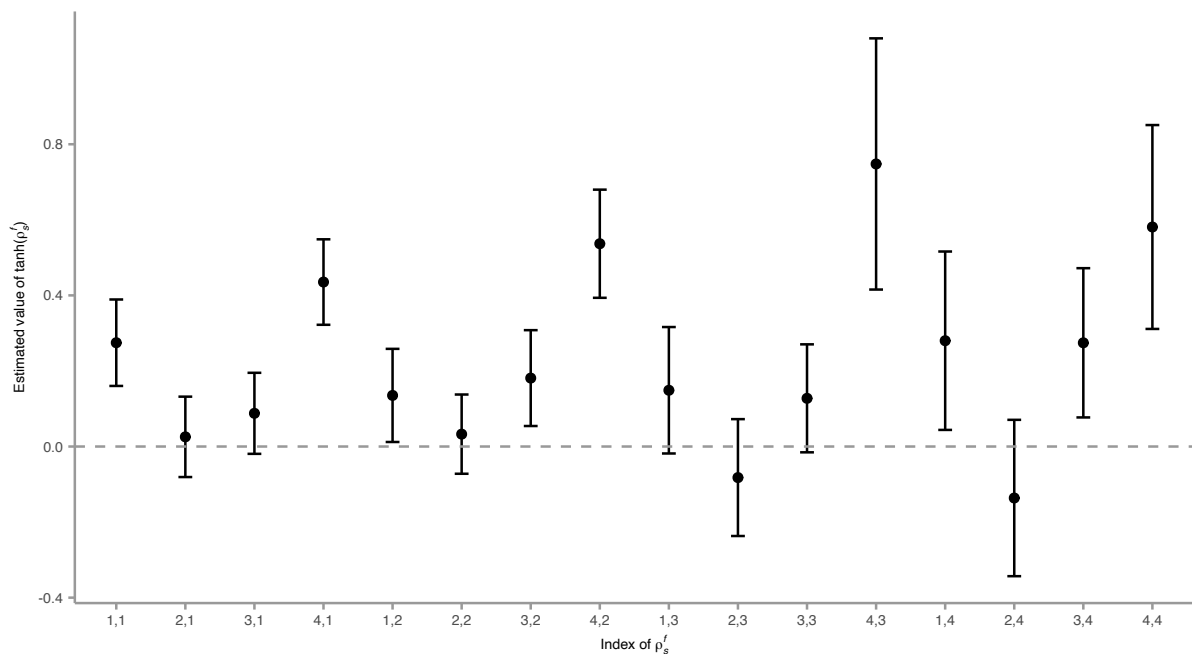
Supporting Figure 1: Parameter estimates quantifying primary ocean-warming effects. The functional form  $\beta_0 + \beta_1(\Delta\text{SST})^2$  incorporating the SST as a predictor variable in the model was for the purpose of parameter estimation recast into  $A + B \times \text{SST} + C \times \text{SST}^2$ , where  $A = \beta_0 + \beta_1\text{SST}_0^2$ ,  $B = -2\beta_1\text{SST}_0$ , and  $C = \beta_1$ . Circles indicate estimated parameter values and error bars the 95 % confidence intervals.



Supporting Figure 2: Parameter estimates quantifying secondary environmental effects. In the model, the parameters associated with explicit predictor variables, here SST, form the vector  $\beta$ , whereas the parameters associated with inferred latent variables form the analogue of the vector  $\beta$ , denoted  $L$ . Circles indicate estimated parameter values and error bars the 95 % confidence intervals.

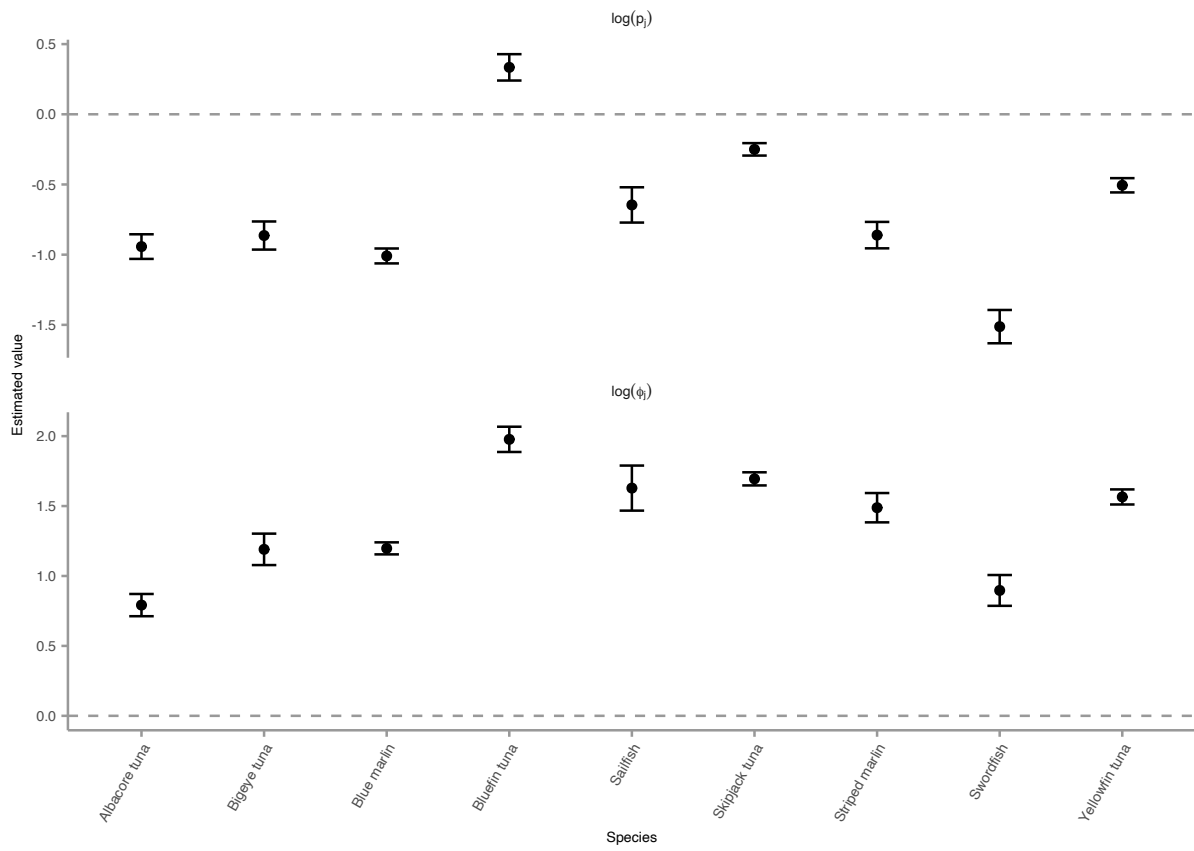


Supporting Figure 3: Parameter estimates quantifying spatial auto-correlation and the resulting covariance functions. (a, b) Circles indicate estimated parameter values and error bars the 95 % confidence intervals. Parameter  $\tau$  determines the variance of the Matérn function via  $\sigma^2 = (4\pi)^{-1}\kappa^{-2}\tau^{-2}$ . (c) The shape of the Matérn covariance functions for each of the four layers comprising the latent spatial field. An important model diagnostic is that the covariance extends beyond the maximum edge distance in the Delaunay triangulation of the study area, represented here by the vertical dashed lines.

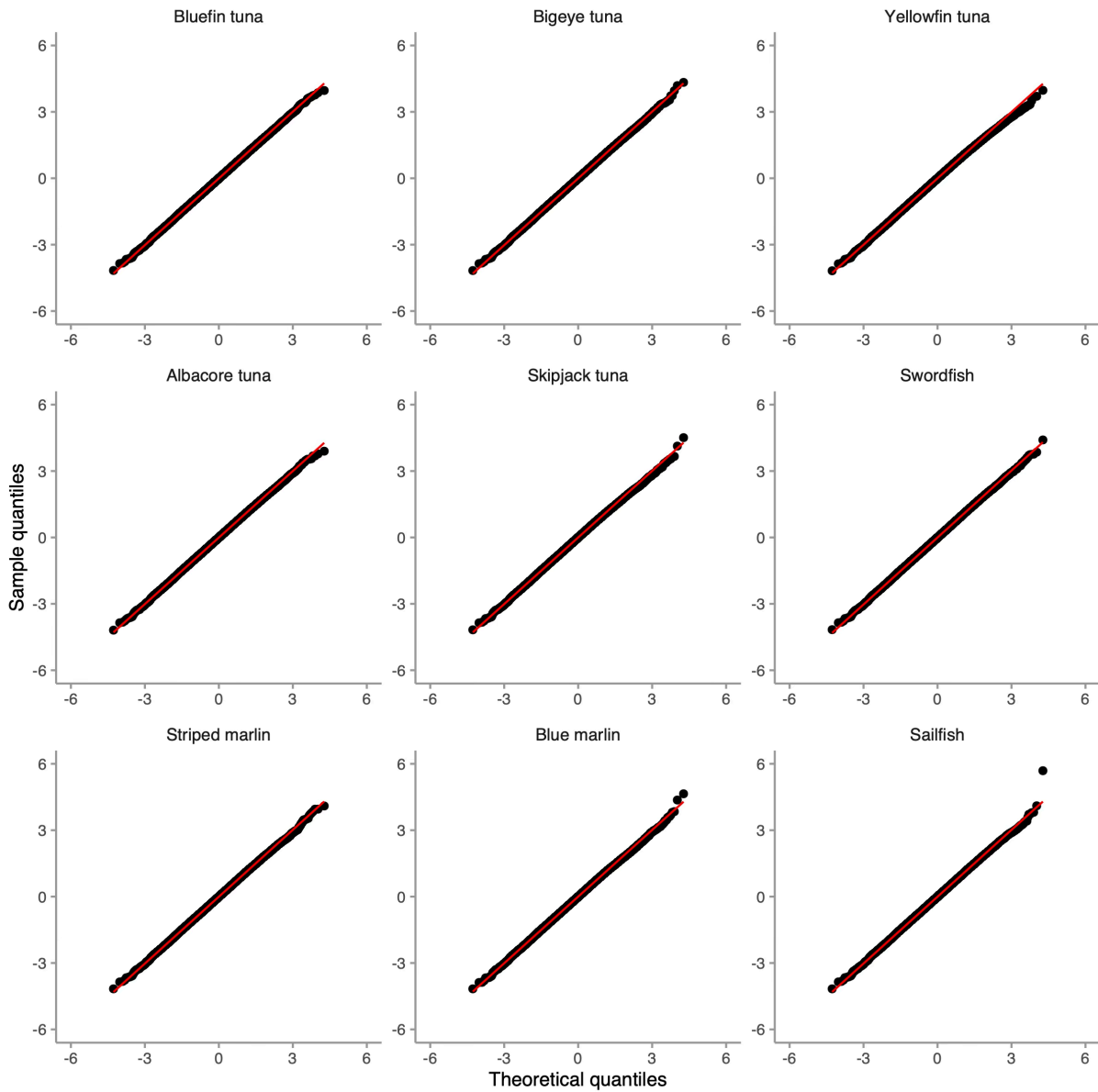


Supporting Figure 4: Parameter estimates quantifying temporal auto-correlation. Circles indicate estimated parameter values and error bars the 95 % confidence intervals. All statistically significant parameters are positive, suggesting that a good season in a given year is likely to be followed by another good season in the next year. Likewise for bad seasons.

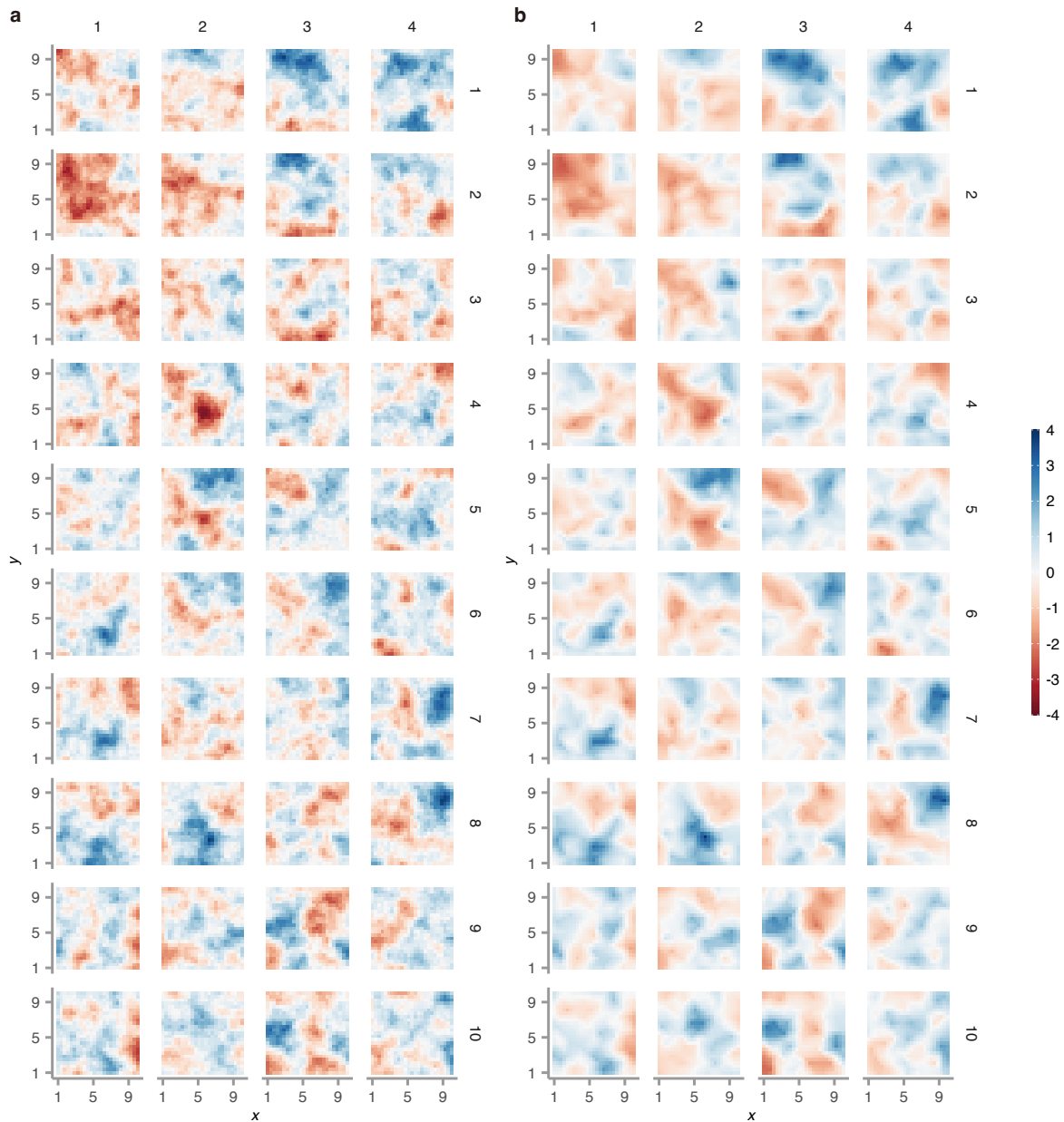




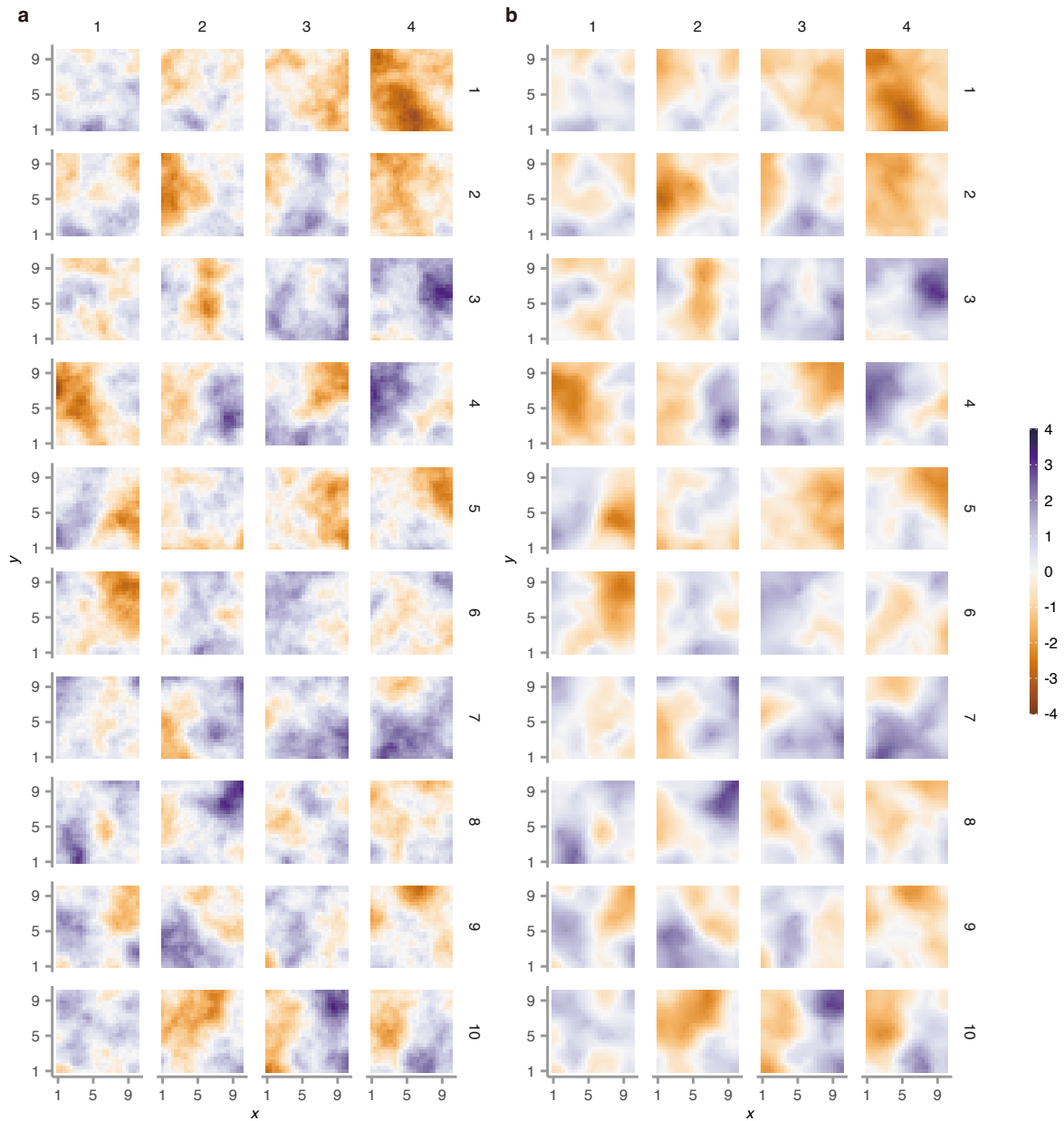
Supporting Figure 5: Parameter estimates for the Tweedie distribution. Circles indicate estimated parameter values and error bars the 95 % confidence intervals.



Supporting Figure 6: Model diagnostics. We calculated randomised quantile residuals (RQRs) because they offer good statistical power and low type I error in detecting misspecification of count regression models, including non-linear covariate effects, over-dispersion, zero inflation, and even misspecified distributional assumptions (*1*). If our model were misspecified, RQRs in the shown Q-Q plots would deviate substantially from the diagonals shown in red. Lack of such deviations implies that the model satisfactorily passed the diagnostic testing against common misspecifications.



Supporting Figure 7: Model diagnostics on an artificial dataset I. We created a 4-season, 10-year long ‘dataset’ by running the model in a configuration with two categorical predictor variables and two layers of the latent spatial field. We then randomly dropped 50% of the data points and fitted the model to the remaining data. (a) The ‘ground-truth’ first layer of the latent spatial field. (b) The model-estimated first layer of the latent spatial field successfully reproduces the features of its ground-truth counterpart. The  $x$  and  $y$  coordinates are in an arbitrary unit of distance. See also Supporting Figure 8.



Supporting Figure 8: Model diagnostics on an artificial dataset II. The same as Supporting Figure 7, but for the second layer of the latent spatial field.

## References

1. Feng, C., Li, L. & Sadeghpour, A. A comparison of residual diagnosis tools for diagnosing regression models for count data. *BMC Med. Res. Methodol.* **20**, 175 (2020).